Water Soluble Melanin Derivatives for Dynamic Contrast Enhanced Photoacoustic Imaging of Tumor Vasculature and Response to Antiangiogenic Therapy

*Dario L. Longo, Rachele Stefania, Chiara Callari, Francesco De Rose, Riccardo Rolle, Laura Conti, Lorena Consolino, Francesca Arena, and Silvio Aime**

Recent advances in nanobiotechnology and nanomaterials are providing novel functional agents that hold great potential in several imaging-based approaches for cancer diagnosis and therapy.[1] Photoacoustic (PA) imaging is a hybrid imaging technique for noninvasive visualization of tissue structures that combine optical excitation with ultrasound detection, exploiting the PA effect.[2] Thanks to the high spatial resolution and imaging depth that this modality can provide, the endogenous PA contrast from naturally occurring tissue cromophores, such as hemoglobin and melanin, allows monitoring anatomic and physiological changes in several diseases as well as following treatment response.[3] Notably, photoacoustic imaging has already been exploited for visualizing human breast cancer based on the intrinsic optical absorption contrast.[4] However, intrinsic PA contrast is usually small and this has prompted the search for exogenous contrast (e.g., organic dyes, quantum dots, carbon nanotubes, gold nanorods, and other platforms) to enhance the role of this imaging modality as diagnostic tool.[5] It has been shown that these agents may markedly improve resolution and sensitivity of PA imaging and the quest for novel materials with improved optoacoustic properties, optimal biodistribution, and low cytotoxicity continues to be under intense scrutiny to expand PA imaging applications.[6] In this context, materials based on naturally occurring biomolecules are receiving great attention due to the obvious biocompatibility they may offer.

Here, we report a novel melanin-based PA contrast agent, as an efficient probe for assessing tumor vasculature properties that allows, for the first time, the setup of a dynamic contrast enhanced (DCE)-PA approach to monitor vascular changes following an antiangiogenic treatment.

Melanin is a natural pigment found widespread in nature including human skin. Dark-brown melanin, or eumelanin, is a macromolecular insoluble structure formed by high-molecular weight polymeric chains with a broad set of biological functions, remarkable for their protective role in oxidative stress, as antioxidant, free radical scavenger, and metal ion storage.[7] Moreover, the broad absorption spectrum of melanin and its good stability in physiological environments makes it well suitable for PA imaging in live animals.[8] Recently, PA probes based on melanin-like nanoparticles have been proposed. These nanoparticles were prepared from synthetic melanin granules dissolved in basic conditions and sonicated to limit aggregation (i.e., to improve their dispersion in aqueous solutions) or by synthesis of artificial melanin models from chemical oxidation of dopamine followed by linear polymerization.[9] As recently pointed out, the capability to control the aggregation state of melanin and hence its solubility is essential for future developments of melanin as functional materials within the PA field.[10] Importantly, melanin-containing nanoparticles can be exploited for multimodality imaging, owing to ability of the melanin macromolecules to chelate metal ions, as well as for drug-loading systems due to its binding capabilities through electrostatic and π–π interactions.[11] However, most of the proposed melanin-like nanoparticles have size that precludes their efficient clearance from the body.[12] Therefore, we adopted a novel strategy for obtaining water soluble melanin derivatives that retain the melanin properties without requiring sonication steps, with dimensions that are optimal in terms of pharmacokinetic and biodistribution within tumors.

Importantly, exogenous agents are commonly exploited in several imaging modalities for assessing tumor microvasculature properties. DCE magnetic resonance imaging is a well established technique that describes the acquisition of baseline images followed by a series of images acquired over time after the intravenous administration of a contrast agent.[13] The characteristic wash-in and wash-out enhancement curves of the contrast agent provide information on the tumor vascular compartment. Notably, DCE is a useful tool for providing early measurement of vascular functional changes after therapeutic treatment and therefore it is considered as a useful biomarker of drug treatment response.[14] In addition, agents with size close to serum albumin can provide a better assessment of tumor vessel permeability and monitor more precisely changes upon antiangiogenic treatments.[15]

In this study, we prepared highly water soluble melanin free-acid (MFA) starting from synthetic melanin granules (sMGs) through a slight modified "bleaching" procedure (**Figure 1**a). sMGs were synthesized by enzymatic (tyrosinase) oxidation of

Dr. D. L. Longo
Institute of Biostructure and Bioimaging (CNR) c/o
Molecular Biotechnology Center
Via Nizza 52, 10126 Torino, Italy
Dr. R. Stefania, Dr. C. Callari, Dr. F. De Rose,
Dr. R. Rolle, Dr. L. Conti, Dr. L. Consolino,
Dr. F. Arena, Prof. S. Aime
Department of Molecular Biotechnology and Health Sciences
University of Torino
Via Nizza 52, 10126 Torino, Italy
E-mail: silvio.aime@unito.it

DOI: 10.1002/adhm.201600550

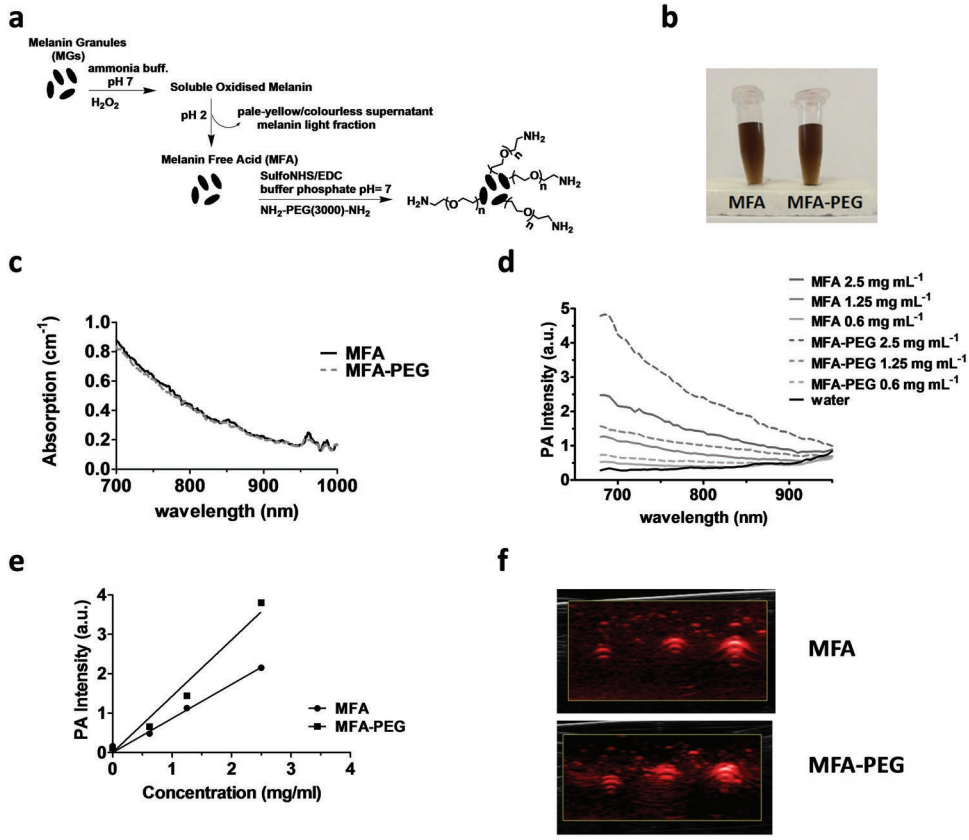

Figure 1. a) Schematic representation of the synthesis of MFA and MFA-PEG. b) Pictures of MFA and MFA-PEG solutions (2.5 mg mL^{-1}) dissolved in H_2O after four months of storage in dark conditions at 4 °C. c) UV–vis absorption and d) PA spectra of MFA and MFA-PEG in 1× PBS at pH = 7.4. e) PA intensities as a function of MFA and MFA-PEG concentrations in PBS. f) Representative PA images of MFA and MFA-PEG solutions in the range of concentrations 0.625–1.25–2.5 mg mL^{-1}, each excited by pulsed laser at 700 nm.

L-dopa.[16] Solubilization of sMG is typically achieved by treatment with hydrogen peroxide in alkaline solution.[17] To remove the solubility-restraining cross-links but still preserving the overall chemical nature of the pigment, we applied a light oxidative breakdown of the melanin structure under mild and neutral pH conditions for a short period of time. Briefly, sMGs were treated with 0.3 M H_2O_2 in 0.12 M ammonia buffer at pH 7 for 20 min at 30 °C. After this mild treatment, the solution phase became markedly dark colored because of the solubilization of sMG that yields the MFA derivative (Figure 1a,b).

The obtained MFA exhibited excellent stability and water solubility up to 10 mg mL^{-1}, with no precipitation after storage at 4 °C for several months (Figure 1b). To further improve dispersibility for applications in living animals, polyethylene glycol (PEG-3000) chains were conjugated to MFA. The MFA-PEG derivative (Figure 1b) has been obtained by a cross-linking reaction between the amine groups of NH_2—PEG_{3000}—NH_2 and the carboxylic groups of MFA. Purification was carried out by gel-filtration chromatography on a Superdex 200 10/300 GL column. The obtained MFA-PEG derivatives maintained the brown-to-black color of the parent MFA (Figure 1b).

Dynamic light scattering (DLS) data showed an average diameter of 6.9 ± 1.2 nm for MFA that reached 10.5 ± 1.8 nm for the PEG-functionalized MFA (Figure S1, Supporting Information). From the point of view of a biological application, small-size systems are expected to be more suitable for biological applications than larger particles, because they are less likely to be rapidly recognized and cleared by macrophages by complement receptor-mediated phagocytosis and they can more easily avoid cellular internalization.[18] The size of MFA-PEG system appears particularly suitable to investigate the wash-in/wash-out process in the tumor region as it is only slightly larger than serum albumin. The similar absorption spectrum of MFA-PEG and MFA demonstrated that the PEG-modification did not influence the absorption properties of MFA and that both MFA and MFA-PEG possess similar optical properties as the parent melanin (Figure 1c).[19]

Stability of MFA nanoparticles in water was assessed by DLS measurements over a period of three months, with no changes in size (Figure S2, Supporting Information). The physiological stability of MFA and MFA-PEG was assessed in cell culture medium (Dulbecco's Modified Eagle Medium, DMEM) and in phosphate-buffered saline (PBS) added of 10% fetal bovine serum, at 37 °C. No changes in PA properties and in absorbance at 700 nm were observed after incubation up to 24 h in both media (Figures S3 and S4, Supporting Information, respectively). Thermostability of MFA and MFA-PEG was assessed upon heating their aqueous solution up to 45 °C. They were found to be stable, since neither precipitation nor significant change in size was detected (Figure S5, Supporting

COMMUNICATION

Information). The overall stability of the MFA and MFA-PEG derivatives was further supported by observing that no significant change occurs in their absorption spectra (Figure S6, Supporting Information) or in their hydrodynamic diameters (Figure S7, Supporting Information) when the pH of their solutions was varied in the range 6.0–7.4. Both MFA and MFA-PEG exhibited negligible photothermal conversion capability (Figure S8, Supporting Information). All together, these data support the view that both MFA and MFA-PEG own a good chemical stability and are therefore well suitable for in vivo applications.

To assess the potential of MFA and MFA-PEG to be used as PA agents, we investigated the detection sensitivity of their aqueous solutions at increasing concentration, from 0.6 to 2.5 mg mL^{-1}. The PA signal increased with the concentration of the MFA and MFA-PEG, with MFA-PEG invariantly showing higher optoacoustic signal intensities at all the investigated wavelengths (Figure 1d). A possible reason for such a higher optoacoustic capability of MFA-PEG in respect to MFA might rely in the higher efficiency of heat transfer between MFA-PEG and water likely due to the PEG coating.[20] MFA and MFA-PEG yield the best PA response, with maximum ultrasound emission, upon excitation at ca. 700 nm value. This wavelength appears well suitable for in vivo work due to the low absorption of deoxygenated blood at this wavelength. In fact, the PA signal generated at ca. 700 nm by a blood sample added of 1.25 mg mL^{-1} MFA and MFA-PEG, respectively, was significantly higher of the one obtained from the neat blood, as shown in Figure S4 (Supporting Information). At higher excitation wavelengths, the MFA containing phantoms display lower PA responses, in comparison to the pure blood sample, reflecting the low PA efficiency of MFA and MFA-PEG at wavelength exceeding 750 nm (Figure 1d). At 700 nm, both MFA and MFA-PEG displayed a linear relationship between PA signal and concentrations (R2 = 0.996 and 0.987 for MFA and MFA-PEG, respectively, Figure 1e). The PA intensity is overlaid with the ultrasound image in Figure 1f, to obtain a tomographic composite image, displaying higher intensities for the MFA-PEG compound.

In vitro tissue culture experiments were used for pilot toxicity studies. The MFA and MFA-PEG were first tested with J774 macrophage cells plated in 96 well plates. Increasing concentrations of MFA and MFA-PEG were added to the culture media and allowed to incubate for 24 h. Analysis by the viability assay indicated no statistically significant decrease in cell viability even at concentrations of 2.5 mg mL^{-1}, for both MFA and MFA-PEG (Figure S9, Supporting Information).

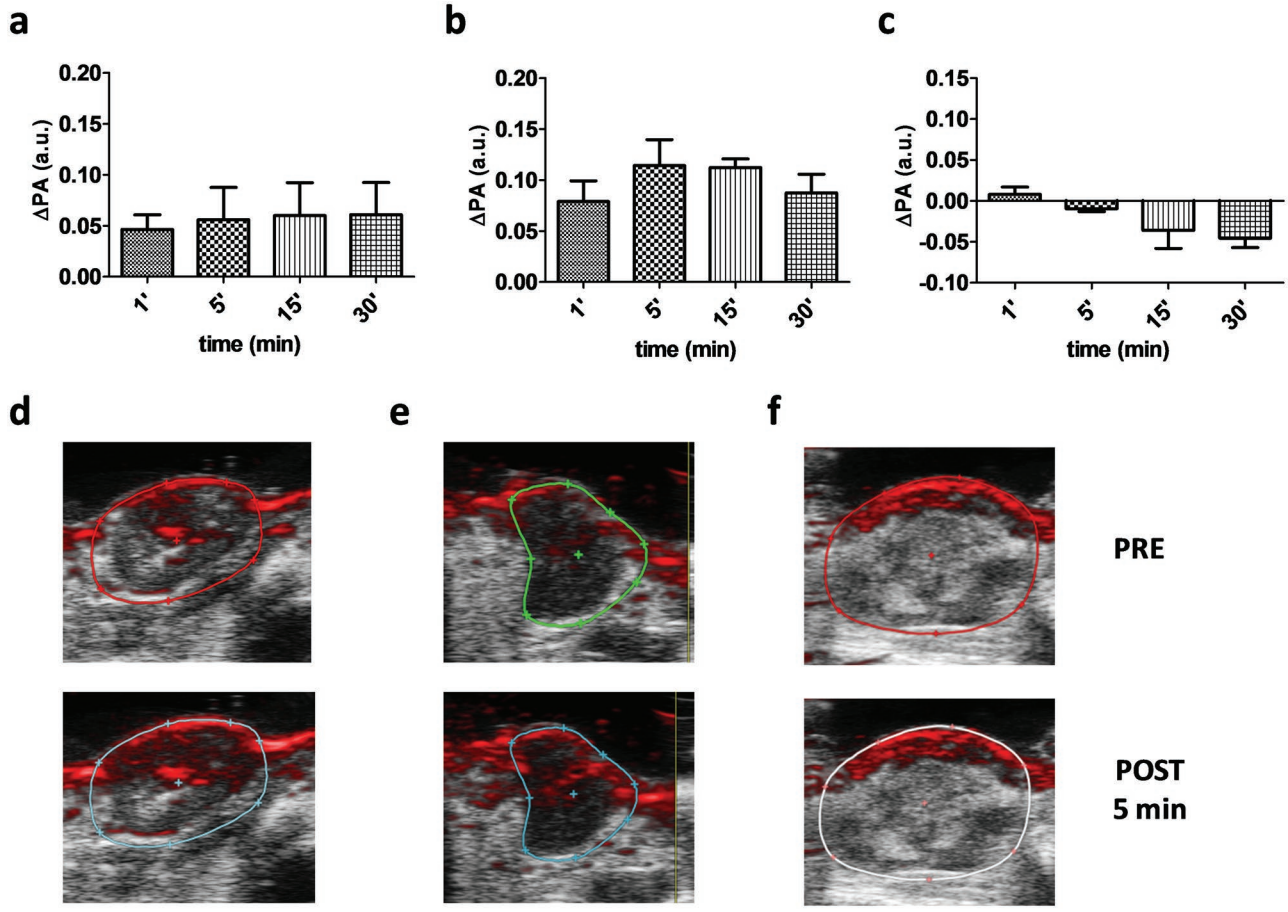

Figure 2. Average PA signal changes upon intravenous administration of 0.1 mL of a) MFA and b) MFA-PEG with concentration of 2.5 mg mL^{-1} or of c) 0.1 mL PBS solution in breast tumor bearing mice ($n = 4$) at 700 nm. Representative optoacoustic images in transverse section of tumor before (top) and 5 min after (bottom) intravenous injection of d) MFA, e) MFA-PEG, and f) PBS at 700 nm. All data are expressed as mean ± SD.

The biodistribution of MFA-PEG was carried out in BALB/c mice bearing a subcutaneous HER2 positive breast tumor generated by injection of ca. 2.5×10^5 TS/A cells. All animal experiments were performed complying with the EU guidelines for the care and use of laboratory animals and with our University Ethical Committee's requirements and according to a protocol approved by the Institutional Animal Care. Mice were injected intravenously with MFA-PEG labeled with a fluorescent dye (S-07186, Ferrania Technologies, Italy), named MFA-PEG-Cy5 (25 µL of 0.06×10^{-3} M MFA-PEG-Cy5 solution) that shows a fluorescence emission peak at 660–670 nm (Figure S10, Supporting Information). The dynamic optical imaging data revealed a rapid distribution and elimination of MFA-PEG-Cy5 in the tumor. Indeed, fluorescent intensity in the tumor reached a high level in the first 5 min after injection of MFA-PEG-Cy5 up to 30 min, followed by a quite fast wash-out (Figures S11 and S12, Supporting Information). MFA-PEG-Cy5 showed a good selectivity for the tumor as a significantly lower signal was detected in the muscle at all time points (Figure S12, Supporting Information). Ex vivo evaluation of organs at 4 h post-injection clearly showed that the highest fluorescence emission was associated with the tumor tissue. MFA-PEG-Cy5 was also found in the liver and the kidneys, the main organs involved in the elimination of the compound, while no specific signal was detected in the heart, lung, spleen, and muscle. In all the organs explanted from control mice treated with the unlabeled compound, a low signal, caused by tissue autofluorescence, was observed (Figure S13, Supporting Information).

The capability of MFA and MFA-PEG for tumor imaging was validated by performing in vivo PA imaging in the HER2 positive TS/A tumor model. Three groups of mice ($n = 4$ for each group) received intravenous administration of 100 µL of a saline solution, or of MFA and MFA-PEG solutions with concentration of 2.5 mg mL^{-1}. After systemic administration of MFA, the PA signal in the tumor gradually increased during the first 30 min, in analogy to what observed in the optical imaging experiments. The average increase, upon subtraction of the baseline PA signal, was in the range 0.05–0.10 a.u. (**Figure 2**a). Upon the systemic administration of MFA-PEG at the same dose, a marked and higher increase of the PA signal was observed in the tumor area, with an average increase between 0.10 and 0.20 a.u. (Figure 2b). The higher contrast enhancement obtained for the MFA-PEG solution likely reflects the enhanced optoacoustic properties of the MFA-PEG in comparison to the MFA compound. Precontrast PA images showed weak PA response in the region of interest, essentially due to the intrinsic absorption of oxyhemoglobin and deoxyhemoglobin in the NIR region (Figure 2d–f). PA images overimposed onto the B-mode images showed a heterogeneous distribution of the signal, with a slight prevalence in the rim region in comparison to the core area (Figure 2d,e). The good PA contrast generated by MFA and MFA-PEG can be accounted in terms of the enhanced permeability and retention effect within tumors. The administration to the control group of the saline solution did not increase at all the PA signal in the first 15 min, with a successive slight reduction (Figure 2c,f). These results give support to the view that the enhanced PA signal in tumor is due to the passive extravasation and accumulation of the MFA and MFA-PEG derivatives.

A further step in tumor characterization is represented by the assessment of tumor vascular permeability. To examine the ability to visualize dynamically tumor vessel permeability, a DCE-PA imaging experiment was performed upon the injection of MFA-PEG into the tail vein. The uptake of MFA-PEG

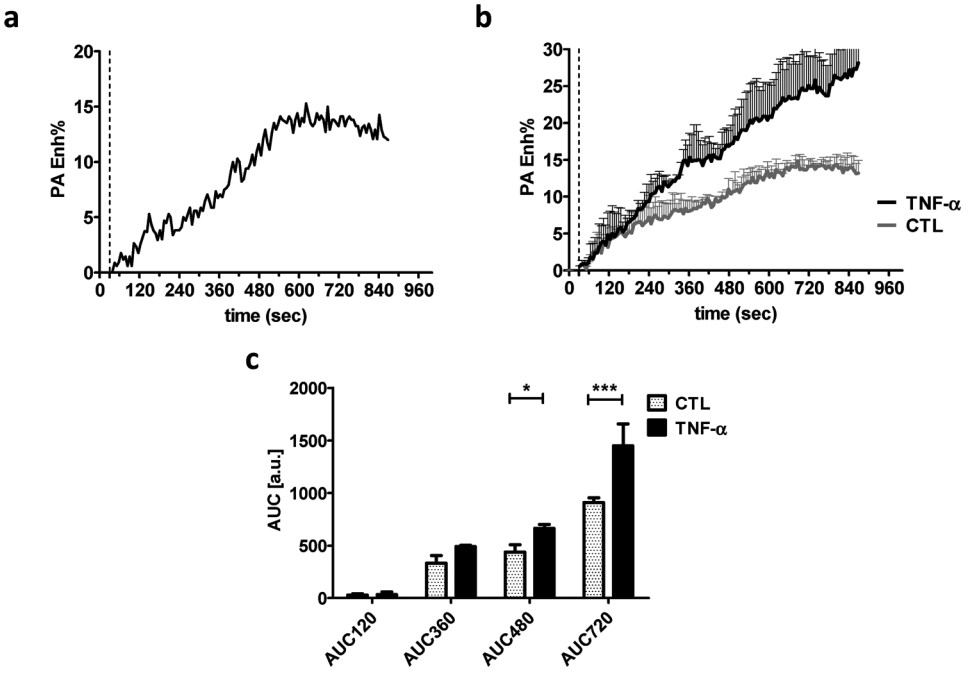

Figure 3. a) Typical time PA intensity curve for intravenous bolus injection of 80 µL of MFA-PEG (2.5 mg mL^{-1}) in the tumor region. b) Averaged dynamic contrast enhanced PA curves (PA Enh%) upon MFA-PEG tail vein injection for control group ($n = 3$) and for TNF-α treated group ($n = 4$). c) Area under the curve (AUC) values at different time points calculated on the corresponding dynamic contrast enhanced curves for control and TNF-α treated mice.

over time was monitored within the tumor region, from which time–intensity PA signal can be extracted and used to describe the microvasculature features (**Figure 3**a). The DCE-PA curve showed a slow but constant uptake into the tumor up to 15 min postinjection. Additionally, to validate the DCE-PA approach for assessing changes in tumor vascularization, we treated a group of mice with tumor necrosis factor-α (TNF-α), an agent used in clinical trials known to increase vascular permeability and uptake of nanosized systems into tumors.[21] Thus, we carried DCE-PA imaging on mice bearing subcutaneous TS/A tumors after intravenous injection of saline solution or of TNF-α. Post-treatment images were acquired after 3 h to allow sufficient time for tumors to respond to TNF-α treatment.[22] Averaged DCE-PA time curves are shown in Figure 3b for control and TNF-α treated group, respectively. As compared to the control group, the PA enhancement curve for the TNF-α group significantly increased upon time after the MFA-PEG injection. To quantify the differences between the two groups, we calculated the area under the curve (AUC) at several time points from the DCE-PA curves. A relatively small increase in AUC values was observed up to 6 min postinjection, which significantly increased from 8 to 12 min (Figure 3c). Clearly the DCE-PA imaging demonstrated that the increase of PA contrast is specific for the enhanced accumulation of MFA-PEG molecules in tumors due to the TNF-α treatment.

In conclusion, we have reported a new synthetic way to produce melanin-based nanosized systems possessing high water solubility as an active platform for PA imaging. These PA nanoscale agents possess relatively small size, good optoacoustic properties, and excellent biocompatibility that point to their use as passive tumor targeting agents. Moreover, for the first time, we showed that these agents can be exploited within a DCE-PA approach for the assessment of changes in tumor vasculature after therapeutic treatment. In addition, owing to the presence of amine moieties on the surface of these particles, one can envisage to exploit these anchoring points for the conjugation of suitable vectors for in vivo active targeting of specific molecular markers.[23]

Supporting Information

Supporting Information is available from the Wiley Online Library or from the author.

Acknowledgements

This work was supported by the Italian Association for Cancer Research (Grant IG 14565) and by the MIUR grant PRIN 2012 (2012SK7ASN).

Received: May 20, 2016
Revised: August 22, 2016
Published online: October 26, 2016

[1] a) K. T. Yong, I. Roy, M. T. Swihart, P. N. Prasad, *J. Mater. Chem.* **2009**, *19*, 4655; b) Y. Liu, H. Miyoshi, M. Nakamura, *Int. J. Cancer* **2007**, *120*, 2527; c) I. Brigger, C. Dubernet, P. Couvreur, *Adv. Drug Delivery Rev.* **2002**, *54*, 631; d) W. H. Chen, C. X. Yang, W. X. Qiu, G. F. Luo, H. Z. Jia, Q. Lei, X. Y. Wang, G. Liu, R. X. Zhuo, X. Z. Zhang, *Adv. Healthcare Mater.* **2015**, *4*, 2247.

[2] a) R. A. Kruger, P. Liu, Y. R. Fang, C. R. Appledorn, *Med. Phys.* **1995**, *22*, 1605; b) V. Ntziachristos, D. Razansky, *Chem. Rev.* **2010**, *110*, 2783; c) L. V. Wang, S. Hu, *Science* **2012**, *335*, 1458; d) R. Su, S. Ermilov, A. Liopo, A. Oraevsky, *Nucl. Instrum. Methods Phys. Res., Sect. A* **2013**, *720*, 58; e) V. Ntziachristos, D. Razansky, *Recent Results Cancer Res.* **2013**, *187*, 133.

[3] a) J. Yao, L. V. Wang, *Contrast Media Mol. Imaging* **2011**, *6*, 332; b) J. Laufer, P. Johnson, E. Zhang, B. Treeby, B. Cox, B. Pedley, P. Beard, *J. Biomed. Opt.* **2012**, *17*, 056016; c) S. E. Bohndiek, L. S. Sasportas, S. Machtaler, J. V. Jokerst, S. Hori, S. S. Gambhir, *J. Nucl. Med.* **2015**, *56*, 1942.

[4] a) J. Menke, *Eur. Radiol.* **2015**, *25*, 2205; b) Z. Xie, F. M. Hooi, J. B. Fowlkes, R. W. Pinsky, X. Wang, P. L. Carson, *Ultrasound Med. Biol.* **2013**, *39*, 2176; c) M. Schwarz, A. Buehler, J. Aguirre, V. Ntziachristos, *J. Biophotonics* **2016**, *9*, 55; d) S. Manohar, S. E. Vaartjes, J. C. G. van Hespen, J. M. Klaase, F. M. van den Engh, W. Steenbergen, T. G. van Leeuwen, *Opt. Express* **2007**, *15*, 12277.

[5] a) G. P. Luke, D. Yeager, S. Y. Emelianov, *Ann. Biomed. Eng.* **2012**, *40*, 422; b) A. De la Zerda, C. Zavaleta, S. Keren, S. Vaithilingam, S. Bodapati, Z. Liu, J. Levi, B. R. Smith, T. J. Ma, O. Oralkan, Z. Cheng, X. Chen, H. Dai, B. T. Khuri-Yakub, S. S. Gambhir, *Nat. Nanotechnol.* **2008**, *3*, 557; c) G. Ku, M. Zhou, S. Song, Q. Huang, J. Hazle, C. Li, *ACS Nano* **2012**, *6*, 7489; d) J. Levi, S. R. Kothapalli, T. J. Ma, K. Hartman, B. T. Khuri-Yakub, S. S. Gambhir, *J. Am. Chem. Soc.* **2010**, *132*, 11264; e) A. V. Liopo, A. Conjusteau, O. V. Chumakova, S. A. Ermilov, R. Su, A. A. Oraevsky, *Nanosci. Nanotechnol. Lett.* **2012**, *4*, 681; f) R. Su, S. A. Ermilov, A. V. Liopo, A. A. Oraevsky, *J. Biomed. Opt.* **2012**, *17*, 101506.

[6] a) K. Pu, J. Mei, J. V. Jokerst, G. Hong, A. L. Antaris, N. Chattopadhyay, A. J. Shuhendler, T. Kurosawa, Y. Zhou, S. S. Gambhir, Z. Bao, J. Rao, *Adv. Mater.* **2015**, *27*, 5184; b) D. Zhang, G. B. Qi, Y. X. Zhao, S. L. Qiao, C. Yang, H. Wang, *Adv. Mater.* **2015**, *27*, 6125; c) X. Zhu, H. Wang, L. Zheng, Z. Zhong, X. Li, J. Zhao, J. Kou, Y. Jiang, X. Zheng, Z. Liu, H. Li, W. Cao, Y. Tian, Y. Wang, L. Yang, *Int. J. Nanomed.* **2015**, *10*, 3719; d) E. V. Petrova, A. A. Oraevsky, S. A. Ermilov, *Appl. Phys. Lett.* **2014**, *105*, 094103; e) S. Manohar, C. Ungureanu, T. G. Van Leeuwen, *Contrast Media Mol. Imaging* **2011**, *6*, 389; f) J. Zeng, M. Cheng, Y. Wang, L. Wen, L. Chen, Z. Li, Y. Wu, M. Gao, Z. Chai, *Adv. Healthcare Mater.* **2016**, *5*, 772.

[7] a) F. P. Noonan, M. R. Zaidi, A. Wolnicka-Glubisz, M. R. Anver, J. Bahn, A. Wielgus, J. Cadet, T. Douki, S. Mouret, M. A. Tucker, A. Popratiloff, G. Merlino, E. C. De Fabo, *Nat. Commun.* **2012**, *3*, 884; b) J. Sedo, J. Saiz-Poseu, F. Busque, D. Ruiz-Molina, *Adv. Mater.* **2013**, *25*, 653.

[8] a) J. B. Dawson, D. J. Barker, D. J. Ellis, E. Grassam, J. A. Cotterill, G. W. Fisher, J. W. Feather, *Phys. Med. Biol.* **1980**, *25*, 695; b) J. Stritzker, L. Kirscher, M. Scadeng, N. C. Deliolanis, S. Morscher, P. Symvoulidis, K. Schaefer, Q. Zhang, L. Buckel, M. Hess, U. Donat, W. G. Bradley, V. Ntziachristos, A. A. Szalay, *Proc. Natl. Acad. Sci. USA* **2013**, *110*, 3316; c) C. X. Qin, K. Cheng, K. Chen, X. Hu, Y. Liu, X. L. Lan, Y. X. Zhang, H. G. Liu, Y. D. Xu, L. H. Bu, X. H. Su, X. H. Zhu, S. X. Meng, Z. Cheng, *Sci. Rep.* **2013**, *3*, 1490.

[9] a) T. Repenko, S. Fokong, L. De Laporte, D. Go, F. Kiessling, T. Lammers, A. J. Kuehne, *Chem. Commun. (Cambridge, UK)* **2015**, *51*, 6084; b) A. Liopo, R. Su, A. A. Oraevsky, *Photoacoustics* **2015**, *3*, 35; c) Q. Fan, K. Cheng, X. Hu, X. Ma, R. Zhang, M. Yang, X. Lu, L. Xing, W. Huang, S. S. Gambhir, Z. Cheng, *J. Am. Chem. Soc.* **2014**, *136*, 15185; d) K. Y. Ju, J. Kang, J. Pyo, J. Lim, J. H. Chang, J. K. Lee, *Nanoscale* **2016**, *8*, 14448.

[10] G. Greco, L. Panzella, G. Gentile, M. E. Errico, C. Carfagna, A. Napolitano, M. d'Ischia, *Chem. Commun. (Cambridge, UK)* **2011**, *47*, 10308.
[11] a) R. P. Zhang, Q. L. Fan, M. Yang, K. Cheng, X. M. Lu, L. Zhang, W. Huang, Z. Cheng, *Adv. Mater.* **2015**, *27*, 5063; b) K. Y. Ju, J. W. Lee, G. H. Im, S. Lee, J. Pyo, S. B. Park, J. H. Lee, J. K. Lee, *Biomacromolecules* **2013**, *14*, 3491.
[12] H. S. Choi, W. Liu, P. Misra, E. Tanaka, J. P. Zimmer, B. Itty Ipe, M. G. Bawendi, J. V. Frangioni, *Nat. Biotechnol.* **2007**, *25*, 1165.
[13] a) N. Hylton, *J. Clin. Oncol.* **2006**, *24*, 3293; b) K. A. Miles, T. Y. Lee, V. Goh, E. Klotz, C. Cuenod, S. Bisdas, A. M. Groves, M. P. Hayball, R. Alonzi, T. Brunner, *Eur. Radiol.* **2012**, *22*, 1430; c) J. M. Hudson, R. Williams, C. Tremblay-Darveau, P. S. Sheeran, L. Milot, G. A. Bjarnason, P. N. Burns, *Eur. J. Radiol.* **2015**, *84*, 1650.
[14] J. P. O'Connor, A. Jackson, G. J. Parker, G. C. Jayson, *Br. J. Cancer* **2007**, *96*, 189.
[15] a) K. Turetschek, A. Preda, V. Novikov, R. C. Brasch, H. J. Weinmann, P. Wunderbaldinger, T. P. Roberts, *J. Magn. Reson. Imaging* **2004**, *20*, 138; b) D. L. Longo, F. Arena, L. Consolino, P. Minazzi, S. Geninatti-Crich, G. B. Giovenzana, S. Aime, *Biomaterials* **2016**, *75*, 47; c) D. L. Longo, W. Dastru, L. Consolino, M. Espak, M. Arigoni, F. Cavallo, S. Aime, *Magn. Reson. Imaging* **2015**, *33*, 725.
[16] T. Sarna, W. Froncisz, J. S. Hyde, *Arch. Biochem. Biophys.* **1980**, *202*, 304.
[17] a) S. Aime, M. Fasano, E. Terreno, C. J. Groombridge, *Pigm. Cell Res.* **1991**, *4*, 216; b) S. Ghiani, S. Baroni, D. Burgio, G. Digilio, M. Fukuhara, P. Martino, K. Monda, C. Nervi, A. Kiyomine, S. Aime, *Magn. Reson. Chem.* **2008**, *46*, 471.
[18] N. Oh, J. H. Park, *Int. J. Nanomed.* **2014**, *9*, 51.
[19] I. A. Vitkin, J. Woolsey, B. C. Wilson, R. R. Anderson, *Photochem. Photobiol.* **1994**, *59*, 455.
[20] Y. S. Chen, W. Frey, S. Aglyamov, S. Emelianov, *Small* **2012**, *8*, 47.
[21] K. W. Chan, T. Yu, Y. Qiao, Q. Liu, M. Yang, H. Patel, G. Liu, K. W. Kinzler, B. Vogelstein, J. W. Bulte, P. C. van Zijl, J. Hanes, S. Zhou, M. T. McMahon, *J. Controlled Release* **2014**, *180*, 51.
[22] S. Folli, A. Pelegrin, Y. Chalandon, X. F. Yao, F. Buchegger, D. Lienard, F. Lejeune, J. P. Mach, *Int. J. Cancer* **1993**, *53*, 829.
[23] a) S. V. Hudson, J. S. Huang, W. Yin, S. Albeituni, J. Rush, A. Khanal, J. Yan, B. P. Ceresa, H. B. Frieboes, L. R. McNally, *Cancer Res.* **2014**, *74*, 6271; b) J. Levi, S. R. Kothapalli, S. Bohndiek, J. K. Yoon, A. Dragulescu-Andrasi, C. Nielsen, A. Tisma, S. Bodapati, G. Gowrishankar, X. Yan, C. Chan, D. Starcevic, S. S. Gambhir, *Clin. Cancer Res.* **2013**, *19*, 1494; c) R. Zhang, D. Pan, X. Cai, X. Yang, A. Senpan, J. S. Allen, G. M. Lanza, L. V. Wang, *Theranostics* **2015**, *5*, 124.